



HAL
open science

Flow through simplified vocal tract geometries

Annemie van Hirtum

► **To cite this version:**

Annemie van Hirtum. Flow through simplified vocal tract geometries. CFA 2010 - 10ème Congrès Français d'Acoustique, Apr 2010, Lyon, France. pp.4. hal-00541379

HAL Id: hal-00541379

<https://hal.science/hal-00541379>

Submitted on 30 Nov 2010

HAL is a multi-disciplinary open access archive for the deposit and dissemination of scientific research documents, whether they are published or not. The documents may come from teaching and research institutions in France or abroad, or from public or private research centers.

L'archive ouverte pluridisciplinaire **HAL**, est destinée au dépôt et à la diffusion de documents scientifiques de niveau recherche, publiés ou non, émanant des établissements d'enseignement et de recherche français ou étrangers, des laboratoires publics ou privés.

10ème Congrès Français d'Acoustique

Lyon, 12-16 Avril 2010

Flow through simplified vocal tract geometries

A. Van Hirtum

Gipsa-lab, UMR CNRS 5216, Grenoble Universities, France

Production of speech utterances such as fricatives involves a complex interaction of turbulent airflow with the particular geometry of the vocal tract. The current study introduces simplified mechanical rigid static vocal tract geometries consisting of a rectangular channel to which 1 or 2 constrictions are inserted allowing to study flow-obstacle and jet-obstacle interaction. Different constriction geometries and constriction degrees are considered. The flow through different geometries is predicted by simplified flow models. Quantitative and qualitative comparison of modelled and measured values is assessed.

1 Introduction

Aero-dynamic and aero-acoustic principles are introduced in speech production studies dealing with fricatives since the sixties [2]. The pioneering work is further developed by experimental as well as modeling studies, *e.g.* [10, 3]. As a result, the underlying mechanism of fricative sound production is well understood as *noise produced due to the interaction of a turbulent jet, produced by a constriction somewhere in the vocal tract, with a downstream wall or obstacle*. Consequently, the position and shape of articulators like tongue and teeth will determine the generation and development of the jet as well as its downstream interaction with a wall or obstacle as is indeed observed on human speakers [6, 8]. Experimental and simulation studies are performed in order to characterise and quantify the influence of articulators position and shape on the sound produced [10, 7]. Nevertheless, the mentioned studies focus on the acoustics of fricative noise production. Therefore, flow data providing a systematic characterisation issuing from configurations relevant to human fricative production, *i.e.* moderate Reynolds Re numbers covering the range $2000 < Re < 10^4$ and low Mach Ma number, are few. Obviously, model validation would benefit from additional flow data providing quantitative information on the flow field as pointed out by *a.o.* [3] in the framework of fricative production. The present study aims to contribute to the systematic study of flow data relevant to describe the jet-obstacle interaction occurring during fricative production.

A rectangular rigid mechanical replica, inspired on the work presented in [10], is proposed in order to mimic the jet-obstacle interaction. The replica consists of a constricted portion between the 'tongue' and the 'palatal plane' upstream of an obstacle representing a 'tooth' for which the constriction can be varied. Its dimensions are taken to be relevant to the human physiology of an 'averaged' male adult vocal tract [6, 8]: length $\approx 180\text{mm}$, unconstricted height $\approx 16\text{mm}$, width $\approx 21\text{mm}$, constriction height between the tongue and the palatal plane $\approx 3\text{mm}$, tooth length $\approx 3\text{mm}$. The gap between the constricted vocal tract portion and the obstacle as well

as the constriction degree at the obstacle are systematically varied. In addition, the flow conditions are varied so that the relevant range of Reynolds numbers is experimentally assessed. The flow is characterised by measuring the volume flow rate and performing point pressure measurements at different positions along the replica. The gathered data are compared to the outcome of one-dimensional flow models commonly used to model the flow in physical models of phonation in order to validate to which degree the applied models are suitable to model the flow through the entire upper airway from the larynx up to the lips. Since it is obvious that the studied flow is too complex to be represented by a laminar flow model, assumed in Bernoulli's equation, several 'ad-hoc' corrections are assessed.

2 One-dimensional flow models

Considering a rectangular channel with two constrictions, see Fig. 1, the total pressure difference ΔP_{tot} is:

$$\Delta P_{tot} = \Delta P_1 + \Delta P_2 + \Delta P_3 + \Delta P_4 + \Delta P_5,$$

with:

$$\begin{aligned}\Delta P_1 &= P(x=0) - P(x=i_1) \\ \Delta P_2 &= P(x=i_1) - P(x=is_1) \\ \Delta P_3 &= P(x=is_1) - P(x=i_2) \\ \Delta P_4 &= P(x=i_2) - P(x=is_2) \\ \Delta P_5 &= P(x=is_2) - P(x=i_3).\end{aligned}$$

It is assumed that no pressure loss occurs in the uniform inlet portion so that $P_0 = P(x=0) = P(x=i_1)$ and $\Delta P_1 = 0$. The pressure losses ΔP_i in the remaining portions with varying area $A_{i,si}$, with subscript i denoting the upstream position and subscript si the downstream position, can be modeled by application of a combination of the following terms from which the pressure distribution $p(x)$ follows immediately [1]:

$$\begin{aligned}\Delta P_i^{ber} &= \phi^2 \frac{\rho}{2} \left(\frac{1}{A_{si}^2} - \frac{1}{A_i^2} \right) \\ &= \phi^2 \frac{\rho}{2} \frac{1}{A_i^2} \left(\frac{A_i^2}{A_{si}^2} - 1 \right)\end{aligned}\quad (1)$$

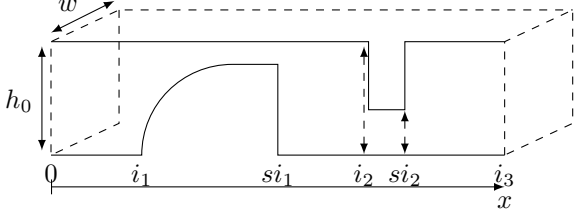


Figure 1: Two-dimensional geometry $h(x)$ with fixed width w . The unstricted channel height is denoted h_0 and two constrictions are inserted, $[i_1 \ s_{i1}]$ and $[i_2 \ s_{i2}]$. The x -axis indicates the main flow direction.

$$\Delta P_i^{pois} = \phi \frac{-12\mu}{w} \int_{x_i}^{x_{si}} \frac{dx}{h(x)^3} \quad (2)$$

$$\begin{aligned} \Delta P_i^{exp} &= \phi^2 \frac{\rho}{2} \frac{1}{A_i^2} \left[\left(\frac{A_i^2}{A_{si}^2} - 1 \right) + \left(1 - \frac{A_i}{A_{si}} \right)^2 \right] \\ &= \phi^2 \frac{\rho}{2} \left[\frac{-2}{A_i A_{si}} \left(1 - \frac{A_i}{A_{si}} \right) \right] \end{aligned} \quad (3)$$

$$\begin{aligned} \Delta P_i^{con} &= \phi^2 \frac{\rho}{2} \frac{1}{A_{si}^2} \left[\left(1 - \frac{A_{si}^2}{A_i^2} \right) + \frac{1}{2} \left(1 - \frac{A_{si}}{A_i} \right) \right] \\ &= \phi^2 \frac{\rho}{2} \frac{1}{A_{si}^2} \left(1 - \frac{A_{si}^2}{A_i^2} \right) \left(1 + \frac{1}{2} \left[1 + \frac{A_{si}}{A_i} \right]^{-1} \right) \end{aligned} \quad (4)$$

$$= \phi^2 \frac{\rho}{2} \frac{1}{A_{si}^2} \left(1 - \frac{A_{si}^2}{A_i^2} \right) \frac{1}{C_{con}^2}, \quad C_{con} < 1 \quad (5)$$

$$\Delta P_i^{ben} = \phi^2 \frac{\rho}{2} \left[\frac{1.1}{A_{si}^2} \left(\frac{2 \cdot 10^5}{Re_D} \right)^{0.2} \right], \quad (6)$$

$$= \phi^2 \frac{\rho}{2} \left[\frac{C_{ben}}{A_{si}^2} \right], \quad Re_D < 2 \cdot 10^5 \rightarrow C_{ben} > 1.1 \quad (7)$$

with volume flux ϕ , mean air density ρ , dynamic viscosity coefficient μ , Reynolds number Re_D based on the corresponding hydraulic diameter which for a rectangular area $A = w \cdot h$ is defined as $Re_D = \frac{2\rho\phi}{\mu(w+h)}$ and the set of corresponding model constants $\{C_{ben}, C_{con}\}$:

$$C_{con} = \left(1 + \frac{1}{2} \left[1 + \frac{A_{si}}{A_i} \right]^{-1} \right)^{-1/2}, \quad (8)$$

$$C_{ben} = 1.1 \left(\frac{2 \cdot 10^5}{Re_D} \right)^{0.2}. \quad (9)$$

For the considered range of Re_D , a typical value of C_{ben} yields $C_{ben} \approx 2.2$.

The first expression (1), denoted ΔP_i^{ber} , assumes a simplified one-dimensional quasi-stationary incompressible and irrotational flow described by the stationary Bernoulli's equation. Several corrections to (1) can be considered due to flow separation, viscosity or downstream pressure recovery. Since steady flow conditions are considered no correction for unsteady flow is necessary. For the geometry shown in Fig. 1 flow separation is assumed to occur at locations x_{si_1} and x_{si_2} regardless upstream pressure P_0 or volume flow rate ϕ so that

the position of flow separation is fixed and no correction for its changing position is needed. Viscous losses, on the contrary, are known to be important in case of low Reynolds numbers, *i.e.* low velocity or small height $h(x)$. Therefore the Bernoulli equation is corrected for viscosity by adding a viscous pressure loss term (2) denoted ΔP_i^{pois} . This term is obtained by assuming a fully developed Poiseuille velocity profile. So far, pressure recovery by flow reattachment upstream the flow separation point is neglected. Pressure recovery is estimated by evaluating the quasisteady momentum equation. The resulting expression (3) describes the pressure recovery as a portion of the Bernoulli loss term (1). The magnitude of the recovery depends on the area ratio A_i/A_{si} at the position of flow separation A_i and the expanded area A_{si} downstream the constriction. It is clear that (3) assumes a uniform flow profile over area A_{si} so that the pressure recovery becomes proportional to $1 - (A_i/A_{si})^2$. On the other hand zero pressure recovery is expected in case a narrow jet flow is assumed to be maintained, so that $A_{si} = A_i$ and the loss term becomes zero since $(1 - A_i/A_{si}) = 0$. In addition to the extreme cases of no recovery or uniform flow, an intermediate value for the pressure recovery is expected when assuming an expanding jet geometry to which (1) can be applied. A geometrical correction for jet expansion is easily obtained by applying an expansion angle θ_{jet} to the uniform narrow jet as:

$$A_{jet} = [h_i + C_{jet} \cdot \tan(\theta_{jet}) \cdot (x_{is} - x_i)] \cdot w, \quad (10)$$

with expansion angle $\theta_{jet} \sim 4.2^\circ$ and model constant C_{jet} set to 1 or 2 accounting for one-side or two-side geometrical expansion of the narrow two-dimensional jet [9].

The constricted portion indicated $[i_2, s_{i2}]$ in Fig. 1 can be seen as a thin square-edged contraction for which separation might occur depending on the Reynolds number at the leading edge, $x = i_2$, instead of the trailing edge, $x = s_{i2}$. In case separation occurs, the flow through the constriction is accelerated and a pressure loss occurs as reported in (5) where C_{con} can be seen as a discharge coefficient whose value can be estimated from geometrical considerations (4), (8) or as an 'ad-hoc' orifice coefficient (5) [1].

The expressions (1) up to (5) assume the main flow direction to be along the x -axis. Although, in particular when the distance between the down- and upstream constriction is reduced, the main flow direction in the gap between both obstacles is likely to be perpendicular to the x -direction. In this case, the geometry can be seen as a sharp 90° bend for which the pressure loss can be described with (7) in which the coefficient C_{ben} is either estimated from the volume flow rate and the geometry (9) or chosen as an 'ad-hoc' bending discharge coefficient [1]. Alternatively, a change in flow direction in the narrowed portion between both constrictions can be simply accounted for by exchanging height and length in this section of the channel and applying the previous mentioned terms, (1) up to (5), in order to determine the pressure distribution $p(x)$ along the main flow direction.

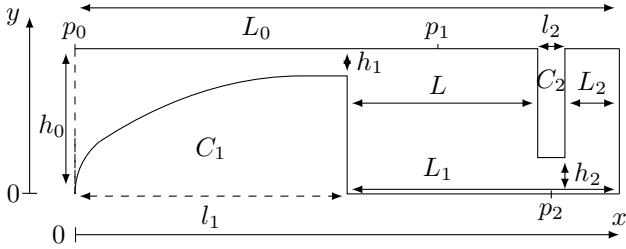


Figure 2: Overview of rigid ‘in-vitro’ replica.

L_1 or L and h_2 [mm]			Constriction degrees [%]	
L_1	L	h_2	$1 - L/h_0$	$1 - h_2/h_0$
-	-	16	0	0
33	24	6.8	0	58
25	16	5.5	0	66
19	10	2.6	38	84
14	5	1.5	69	91
12	3	0.6	81	96
1	-	-	-	-

Table 1: Assessed geometrical configurations.

3 Mechanical replica and setup

The rigid ‘in-vitro’ replica consists of two constrictions, C_1 and C_2 , inserted in a uniform rectangular channel as schematically depicted in Fig. 1 and detailed in Fig. 2. The unstricted channel has length $L_0 = 180\text{mm}$, height $h_0 = 16\text{mm}$, width $w = 21\text{mm}$ and aspect ratio $w/h_0 = 1.3$. The shape of both constrictions C_1 and C_2 is fixed. Their lengths in the x -direction yield $l_1 = 30\text{mm}$ for C_1 and $l_2 = 3\text{mm}$ for C_2 . The aperture h_1 is fixed to 3mm , which corresponds to a constriction degree of 81% . The distance of the trailing edge of C_2 to the channel exit, L_2 , is fixed to 6mm . The distance of the trailing edge of C_1 with respect to the channel exit, L_1 , can be varied as well as aperture height h_2 of constriction C_2 . Therefore, besides the inlet height h_0 , the pressure distribution is determined by the set of geometrical parameters $\{h_1, L_1, h_2\}$ of which L_1 and h_2 can be varied. In order to validate the pressure drop three pressure taps are assessed at positions $p_0 = 30\text{mm}$, $p_1 = 160\text{mm}$ and $p_2 = 173\text{mm}$ from the channel inlet. Experimentally assessed combinations of $\{L_1, h_2\}$ are summarised in Table 1 and schematically illustrated in Fig. 3. Since the position of the pressure tap p_1 is fixed, p_1 is situated in the gap between C_1 and C_2 for large L_1 or along C_2 in case L_1 is closer to the channel exit.

4 Flow and pressure data

The geometrical configurations depicted in Fig. 2 and Fig. 3 are assessed for upstream pressures $P_0 < 4000\text{Pa}$. The associated bulk Reynolds numbers, defined as $Re = \phi/(\nu w)$, are $Re \in [0, 15000]$. Fig. 4 shows the measured values of Re and downstream pressures (P_1, P_2) as function of P_0 and the geometrical parameters (L_1, h_2).

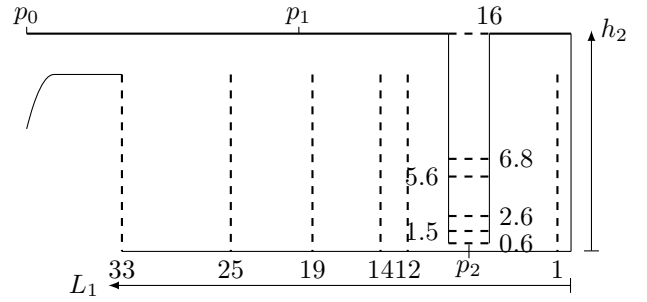


Figure 3: Assessed geometrical configurations.

Fig. 4(a) illustrates the measured relationship $Re(P_0)$. For $h_2 = 0.6\text{mm}$ corresponding to a constriction degree of 96% the relationship $Re(P_0)$ is seen to be nearly independent of L_1 since the relative difference is inferior to 5% for all assessed volume airflows. For $h_2 = 1.5\text{mm}$ the presence of both constrictions becomes notable since increasing L_1 from 12 to 33mm slightly decreases P_0 with 8% and further down to 12% in absence of C_1 . The same tendency is observed more clearly as the aperture h_2 is further increased. The relative pressure decrease with increasing L_1 from 12 down to 33mm yields 25% , 44% and 51% for $h_2 = 2.6$, $h_2 = 5.5$ and $h_2 = 6.8\text{mm}$ and decreases further to 38% , 78% and 87% in absence of C_1 . Consequently, the pressure drop increases when the gap between both constrictions is narrowed indicating that pressure recovery is favored in case of a wide gap between both constrictions.

In absence of C_2 , *i.e.* $h_2 = h_0 = 16\text{mm}$, pressure recovery is mainly determined by constriction degree of 81% due to the fixed aperture of $h_1 = 3\text{mm}$. Consequently, varying L_1 from 33 up to 1mm results in a fairly constant pressure drop P_0 regardless the volume airflow rate. The slight pressure increase, inferior to 4% , for increasing L_1 is the result of a small pressure recovery in the channel. Fig. 4(b) illustrates the pressures measured at p_1 normalised to the upstream pressure, P_1/P_0 . As illustrated in Fig. 3 the relative position of the pressure tap p_1 with respect to the trailing edge of constriction C_1 depends on L_1 . From Fig. 4(b) it is seen that in absence of C_1 the pressure ratio P_1/P_0 collapses to a single curve, which is independent from h_2 and the volume airflow velocity ϕ . Nevertheless, the pressure loss is increasing with input pressure up to 30% firstly due to friction since the friction factor is Reynolds number dependent and secondly due to the development of entry flow in the uniform inlet portion of the channel with length 13cm [4]. In addition, since the aspect ratio $h_0/w = 1.3 \approx 1$, three-dimensional flow development is likely to occur [9]. Inserting constriction C_1 in absence of constriction C_2 , *i.e.* $h_2 = h_0 = 16\text{mm}$, leads to a pressure drop as expected from the terms discussed in section 2. For $L_1 = 1$ up to $L_1 = 33\text{mm}$ the pressure tap p_1 is situated consecutively along the converging portion of C_1 , at the minimum constriction and finally in the gap between both constrictions, so that the associated pressure drop is seen to increase from $\pm 40\%$ up to $\pm 100\%$, *i.e.* $P_1 \approx 0$. The pressure drop P_1/P_0 measured in presence of both constrictions C_1 and C_2 is intermediate to the previous configurations: a lower limit is reached in absence

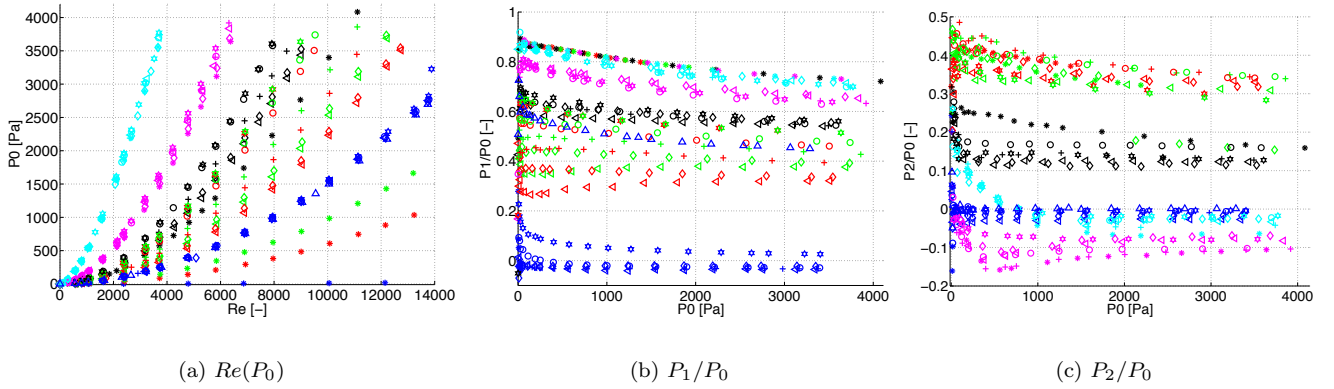


Figure 4: Overview of experimental results of $Re(P_0)$, $P_1/P_0(P_0)$ and $P_2/P_0(P_0)$ for all assessed geometrical (L_1, h_2) and flow (P_0) configurations: absence of the downstream obstacle C_1 is indicated as $L_1 = \text{none}$ (*), $L_1 = 33$ (\triangleright), $L_1 = 25$ (\diamond), $L_1 = 19$ (+), $L_1 = 14$ (\circ), $L_1 = 12$ (\star), $L_1 = 1\text{mm}$ (\triangle), $h_2 = 16$ (blue), $h_2 = 6.8$ (red), $h_2 = 5.5$ (green), $h_2 = 2.6$ (black), $h_2 = 1.5$ (magenta) and $h_2 = 0.6\text{mm}$ (cyan).

of C_1 and an upper limit in absence of C_2 . As for $Re(P_0)$ shown in Fig. 4(a) the influence of L_1 on pressure P_1 is most noticeable for large $h_2 > h_1 = 3\text{mm}$, *i.e.* 6.8 and 5.5mm, for which the pressure loss is seen to decrease with 12% or more as the gap L_1 becomes wider. In addition, the pressure loss P_1/P_0 measured for $h_2 > h_1 = 3\text{mm}$ is more pronounced as for smaller h_2 , *i.e.* $h_2 \leq h_1 = 3\text{mm}$, for which the pressure loss $P_1/P_0 > 0.5$. Consequently, the relative pressure drop P_1/P_0 reduces as h_2 decreases since the pressure drop across C_2 is increasing.

From the previous discussion of measured P_1/P_0 values and from the model terms presented in section 2, accounting for pressure recovery in the gap between both constrictions is expected to be important for h_2 in the range $h_0 > h_2 > h_1$ and much less for $h_2 < h_1$. Fig. 4(c) reports measured pressure losses P_2/P_0 observed at pressure tap p_2 . The pressure drop for C_2 is most important for small apertures h_2 resulting in negative pressures for $h_2 \leq 1.5\text{mm}$ with an order of magnitude about 10% of P_0 . Nevertheless, the pressure drop is more pronounced for $h_2 = 1.5\text{mm}$ than for $h_2 = 0.6\text{mm}$. This might be due 1) to viscosity as seen from (2), 2) a consequence of the strong asymmetry resulting in a downstream shift of the minimum pressure [5] or 3) related to a small recirculation zone at the position p_2 . Varying L_1 is seen to influence P_2/P_0 in particular for small apertures $h_2 \leq 1.5\text{mm}$ for which the presence of C_1 is seen to decrease the pressure drop for the assessed flow conditions.

5 Validation of 1D flow models

The pressure distribution is estimated from models taking into account different terms, (1) up to (7), as discussed in section 2. Resulting models q and their principle features are summarised in Table 2. The assessed geometry and the total pressure difference corresponding to the measured upstream pressure, *i.e.* assuming $\Delta P = P_0$, are model input parameters from which the volume airflow velocity and pressure distribution along the ‘in-vitro’ replica geometry, parameterised by

q	Model terms of section 2					terms
	(1)	(2)	(3)	(4)	(6)	
Ber	×					Bernoulli
Poi	×	×				viscosity
Exp			×			expansion
Con				×		contraction
Ben					×	bending

Table 2: Overview models formulated with terms (1) up to (7). For each model q , the terms taken into account are indicated by \times .

(L_1, h_2) , are estimated.

Model estimations of the volume airflow velocity and of the pressures at the positions of the pressure taps, *i.e.* \hat{P}_1 , \hat{P}_2 and $\hat{\phi}$, can be quantitatively compared to experimentally observed values for each set of input parameters (P_0, L_1, h_2) in order to determine the model accuracy. Consequently, the accuracy of the model estimations for \hat{P}_1 , \hat{P}_2 and $\hat{\phi}$ is sought as function of (P_0, L_1, h_2) for each model q . Relative error functions $\zeta_1^{(q)}(\hat{P}_1, P_0, L_1, h_2)$, $\zeta_1^{(q)}(\hat{P}_2, P_0, L_1, h_2)$ and $\zeta_2^{(q)}(\hat{\phi}, P_0, L_1, h_2)$ are obtained for each model, denoted by superscript q , as:

$$\zeta_1^{(q)}(\hat{P}_m, P_0, L_1, h_2) = \frac{|\hat{P}_m - P_m|}{P_0}, \text{ with } m \in \{1, 2\} \quad (11)$$

$$\zeta_2^{(q)}(\hat{\phi}, P_0, L_1, h_2) = \frac{|\hat{\phi} - \phi|}{\phi}, \quad (12)$$

where as before P_0 , P_m and ϕ indicate the measured values. An error function $\bar{\zeta}_k^{(q)}$ for all $N_0(L_1, h_2)$ assessed P_0 -values is defined as:

$$\bar{\zeta}_k^{(q)}(\cdot, L_1, h_2) = \frac{1}{N_0} \sum_{r=1}^{N_0} \left(\zeta_k^{(q)}(\cdot, P_{0_r}, L_1, h_2) \right), \quad (13)$$

for which the summation index r in P_{0_r} sums over all N_0 assessed P_0 values for each geometrical configuration (L_1, h_2) whereas $\zeta_k^{(q)}$ as well as the variable \cdot are

defined by (11) for $k = 1$ ($\cdot = P_m$) and (12) for $k = 2$ ($\cdot = \phi$). From (13) the overall best mean model error $\bar{\zeta}^{(\hat{q})}(L_1, h_2)$ with respect to all assessed models q is than straightforwardly quantified as the model \hat{q} minimising the cost function $J(q)$ as expressed in (14) and (15):

$$J(q, L_1, h_2) = \frac{1}{3} \left(\bar{\zeta}_1^{(q)}(\hat{P}_1, L_1, h_2) + \bar{\zeta}_1^{(q)}(\hat{P}_2, L_1, h_2) + \bar{\zeta}_2^{(q)}(\hat{\phi}, L_1, h_2) \right), \quad (14)$$

$$\hat{q}(L_1, h_2) = \arg \min_q J(q, L_1, h_2). \quad (15)$$

The overall best mean model errors $J(\hat{q}, L_1, h_2)$ are plotted in Fig. 5. Fig. 6 depicts the corresponding averaged errors $\bar{\zeta}_k^{(\hat{q})}(\cdot, L_1, h_2)$ (13) for \hat{P}_1 , \hat{P}_2 and $\hat{\phi}$. In addition to the error values (13), the errorbars in Fig. 6 illustrate the sensitivity of the model accuracy for variations of the upstream pressure P_0 . In general, the error sensitivity increases as the error values $\bar{\zeta}_k^{(\hat{q})}(\cdot, L_1, h_2)$ increases. The overall best mean model error yields

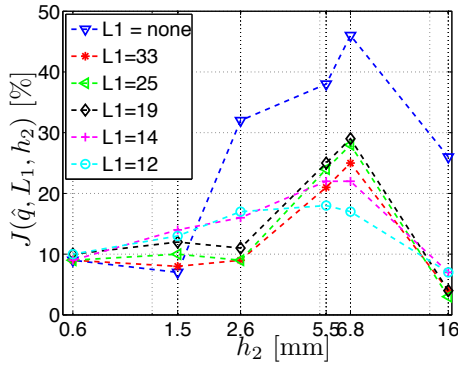


Figure 5: Overall best mean model error $J(\hat{q}, L_1, h_2)$ (14) of the models $\hat{q}(L_1, h_2)$ summarised in Table 3 versus h_2 as function of L_1 . Absence of the downstream obstacle C_1 is denoted $L_1 = \text{none}$.

$J(\hat{q}, L_1, h_2) < 30\%$ for all (L_1, h_2) except in absence of C_1 , denoted $L_1 = \text{none}$. In absence of C_1 , the errors for $h_2 > 1.5$ are significantly larger than in presence of C_1 , so that the upper limit for the overall model accuracy increases to $J(\hat{q}, L_1, h_2) < 50\%$. From Fig. 6 is observed that in presence of C_1 large overall errors $J(\hat{q}, L_1, h_2)$, e.g. $h_2 = 5.5$ compared to $h_2 = 1.5$ in Fig. 5, are due to large errors of $\bar{\zeta}_1^{(\hat{q})}(\hat{P}_2, L_1, h_2)$ and/or $\bar{\zeta}_2^{(\hat{q})}(\hat{\phi}, L_1, h_2)$. In absence of C_1 , the error $\bar{\zeta}_1^{(\hat{q})}(\hat{P}_1, L_1, h_2)$ is seen to increase as well explaining the increased overall best mean error upper limit of $J(\hat{q}, L_1, h_2) < 50\%$ instead of $J(\hat{q}, L_1, h_2) < 30\%$.

The models resulting in the overall best mean model error $J(\hat{q}, L_1, h_2)$ (14), illustrated in Fig. 5, are summarised in Table 3. From Table 3 is seen that for $h_2 = 16$ as well as $h_2 = 0.6$ accounting for viscous effects, i.e. $\hat{q} = \text{Poi}$, results in the sought errors $J(\hat{q}, L_1, h_2)$ regardless the value of L_1 . For intermediate values, $0.6 < h_2 < 16$, the overall best mean model errors $J(\hat{q}, L_1, h_2)$ are obtained for models $\hat{q} = \text{Con}$ or $\hat{q} = \text{Ben}$ depending on (L_1, h_2) . It is observed that inserting L_1 upstream from h_2 and moving it further

downstream, i.e. decreasing L_1 , causes a model shift from $\hat{q} = \text{Con}$ to $\hat{q} = \text{Ben}$. So, in case of a large gap L_1 between both constrictions C_1 and C_2 , the narrowed passage at C_2 can be modelled as a sudden constriction whereas for smaller L_1 the narrowed passage C_2 can be approximated as a bend in the geometry. The transition, i.e. constriction \rightarrow bending, is seen to depend on the value of the aperture h_2 .

6 Conclusion

A rigid ‘in-vitro’ replica is proposed in order to study airflow through the human vocal tract during fricative production. Two geometrical parameters are experimentally studied: the position of an upstream ‘tongue’ shaped constriction in the main flow direction (L_1) and the constriction degree of a ‘tooth’ shaped downstream obstacle (h_2). The shape of both obstacles is extremely simplified in order to limit the number of geometrical and flow parameters to be taken into account.

Point pressure measurements (11mm upstream and at the ‘tooth’ constriction) vary significantly over the range of imposed L_1 and h_2 . In addition, varying L_1 while maintaining h_2 fixed is seen to influence the pressure at the ‘tooth’ constriction. Consequently, besides h_2 , L_1 influences the resulting airflow.

Measured pressures and volume airflow rates are compared to the outcome of one-dimensional flow models assuming a laminar incompressible irrotational and one-dimensional flow governed by Bernoulli equation to which corrections are applied for viscosity, sudden geometrical expansion, sudden geometrical constriction and a bending geometry. In presence of the ‘tongue’ shaped constriction, the accuracy for each set of geometrical parameters (L_1, h_2) expressed as a mean error for all predicted quantities and all imposed upstream pressures yields $< 30\%$. The model resulting in the minimum errors varies as function of (L_1, h_2) . For very small ($\leq 58\%$) or very large ($\geq 96\%$) constriction degrees at the ‘tooth’ the most accurate model is obtained by accounting for viscosity regardless the value of L_1 . For intermediate constriction degrees, in the interval $[58, 96]\%$, narrowing the gap between both constrictions, i.e. decreasing L_1 , causes the most accurate model to shift from constriction to bending. Therefore, the geometrical parameter L_1 , although not explicitly appearing as a parameter in the validated one-dimensional models, does determine the appropriate corrective term in terms of the applied cost function. In addition, it is interesting to note that the best model accuracy is poorest for ‘tooth’ constriction degrees ($\approx 60\%$) for which the influence of L_1 on the measured pressures is most significant. Consequently, one-dimensional flow models can be applied to describe the flow through the vocal tract when accounting for the relevant corrections in order to compensate, on geometrical considerations, for the non realistic assumption of a laminar and irrotational flow. This way the approach of one-dimensional flow modeling, commonly used in physical phonation models, can be extended to the vocal tract. Nevertheless, several topics for further research can be formulated. With respect to modelling, more complex flow modeling is moti-

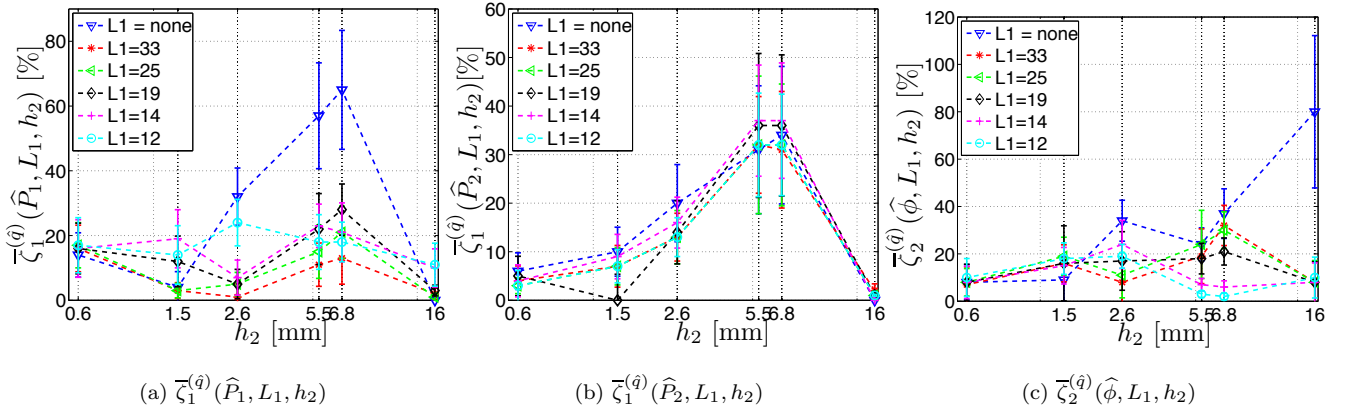


Figure 6: Model errors $\bar{\zeta}_k^{(\hat{q})}(\cdot, L_1, h_2)$ (13) for \hat{P}_1 , \hat{P}_2 and $\hat{\phi}$ for the models $\hat{q}(L_1, h_2)$ corresponding to $J(\hat{q}, L_1, h_2)$ presented in Fig. 5 and summarised in Table 3 versus h_2 as function of all assessed L_1 : a) $\bar{\zeta}_1^{(\hat{q})}(\hat{P}_1, L_1, h_2)$, b) $\bar{\zeta}_1^{(\hat{q})}(\hat{P}_2, L_1, h_2)$ and c) $\bar{\zeta}_2^{(\hat{q})}(\hat{\phi}, L_1, h_2)$. Absence of the downstream obstacle C_1 is denoted $L_1 = \text{none}$.

			Decreasing L_1						
$\vartheta_1(L_1)$			0	0	0	38	69	81	
	$\vartheta_2(h_2)$	$h_2 \setminus L_1$	$L_1 = \text{none}$	$L_1 = 33$	$L_1 = 25$	$L_1 = 19$	$L_1 = 14$	$L_1 = 12$	terms
Decreasing h_2	0	16	Poi	Poi	Poi	Poi	Poi	Poi	viscosity
	58	6.8	Con	Ben	Ben	Ben	Ben	Ben	constriction \rightarrow bending
	66	5.5	Con	Con	Con	Ben	Ben	Ben	constriction \rightarrow bending
	84	2.6	Con	Con	Con	Con	Con	Ben	constriction \rightarrow bending
	91	1.5	Con	Ben	Ben	Ben	Ben	Ben	constriction \rightarrow bending
	96	0.6	Poi	Poi	Poi	Poi	Poi	Poi	viscosity

Table 3: Overview of the selected models $\hat{q}(L_1, h_2)$ resulting in the overall best mean error $J(\hat{q}, L_1, h_2)$ (14) whose value is plotted in Fig. 5. Models are referred to as outlined in Table 2. For completeness also the constriction degree due to h_2 , *i.e.* $\vartheta_2(h_2) = 1 - h_2/h_0$ [%], and the constriction degree of the gap between both constrictions due to L_1 , *i.e.* $\vartheta_1(L_1) = 1 - (L_1 - 9)/h_0$ [%], are indicated as well.

vated in order to describe the influence of the geometrical parameter L_1 . In addition, further flow and acoustic experimental characterisation needs to be assessed either qualitative (flow visualisation) or/and quantitative (Particle Image Velocimetry, anemometry, microphone).

Acknowledgments

Financial support of the Agence Nationale de la Recherche is gratefully acknowledged.

References

- [1] R. Blevins. *Applied Fluid Dynamics Handbook*. Krieger publishing company, Malabar, 1992.
- [2] G. Fant. *The acoustic theory of speech production*. Mouton, The Hague, 1960.
- [3] M. Howe and R. McGowan. Aeroacoustics of [s]. *Proc. R. Soc. A*, 461:1005–1028, 2005.
- [4] A.K. Kapila, G.S.S. Ludford, and V.O.S. Olunloyo. Entry flow in a channel. part 3. inlet in a uniform stream. *J. Fluid Mechanics*, 57(1):769–784, 1973.
- [5] P.Y. Lagr e, A. Van Hirtum, and X. Pelorson. Asymmetrical effects in a 2D stenosis. *European Journal of Mechanics B/Fluids*, 26:83–92, 2007.
- [6] S. Narayanan, A. Alwan, and K. Haker. An articulatory study of fricative consonants using magnetic resonance imaging. *J. Acoust. Soc. Am.*, 98:1325–1347, 1995.
- [7] G. Ramsay. The influence of constriction geometry on sound generation in fricative consonants. In *Proc. Acoustics08*, pages 1–4, Paris, France, 2008.
- [8] C. Runte, M. Lawerino, D. Dirksen, F. Bollmann, A. Lamprecht-Dinnesen, and E. Seifert. The influence of maxillary central incisor position in complete dentures on /s/ sound production. *The journal of prosthetic dentistry*, 85:485–495, 2001.
- [9] H. Schlichting and K. Gersten. *Boundary layer theory*. Springer Verlag, Berlin, 2000.
- [10] C. Shadle. *The acoustics of fricative consonants*. PhD thesis, 1985.